Journal of Alloys and Compounds 509 (2011) 9428–9433

Contents lists available at ScienceDirect

Journal of Alloys and Compounds

journal homepage: www.elsevier.com/locate/jallcom

Low-temperature solid-state synthesis and optical properties of CdS–ZnS and ZnS–CdS alloy nanoparticles

Jinsong Liu[a,*], Chuanbao Zhao[a], Ziquan Li[a], Jiankang Chen[a], Hengzhi Zhou[b], Shanqun Gu[a], Youhong Zeng[a], Yongchan Li[a], Yongbing Huang[b]

[a] College of material science and technology, Nanjing university of aeronautics and astronautics, Nanjing, Jiangsu 210016, China
[b] Department of materials science and engineering, Nanjing institute of technology, Nanjing, Jiangsu 211167, China

ARTICLE INFO

Article history:
Received 13 January 2011
Received in revised form 29 June 2011
Accepted 2 July 2011
Available online 23 July 2011

Keywords:
Chemical synthesis
Semiconductors
Optical properties
Formation mechanism

ABSTRACT

A simple low-temperature solid-state synthetic method was employed to obtain ZnS–CdS and CdS–ZnS alloy nanoparticles. The effects of reaction sequence, reactant molar ratios, and synthesis temperature on the products were investigated. The crystal structure and morphology of the products were characterized by X-ray diffraction (XRD), transmission electron microscopy (TEM), and fourier transform infrared (FT-IR) spectroscopy. The results show that the products are alloy nanoparticles with a cubic phase structure. The formation mechanism of the alloy nanoparticles is briefly discussed. Sufficient grinding and crystalline water may be essential to form alloy nanoparticles. Ultraviolet–visible (UV–vis) spectra show that the edge absorptions of the CdS–ZnS and ZnS–CdS nanoparticles were located between those of ZnS and CdS bulks, and the absorbance at the peak maximum was practically dependent on reaction temperature, reaction sequence, and molar ratio. Extrinsic deep-level emission resulted in strong peaks in the photoluminescence (PL) spectra. The position and intensity of the emission peaks varied with the conditions during synthesis.

1. Introduction

In the past decades, many efforts have been focused on groups II–VI semiconductor nanomaterials due to their unique properties and potential applications in electrical, optoelectronic, and photochemical fields. Continuous research suggests that semiconductor/semiconductor nanocomposites confer a noticeable enhancement in the luminescence and conductive properties due to elimination of surface non-radiative recombination defects [1–4]. Therefore, the design and preparation of composite nanomaterials, such as CdSe/ZnS, CdSe/CdS, and ZnO/ZnS have been attracted much more research interests [5–7].

ZnS and CdS, as group II–VI semiconductor materials with wide band gap, are commercially used as the phosphors in thin-film electroluminescent devices, solar cells, and other optical electronic devices [8–11]. Their nanocomposites are being extensively studied due to their good semiconductor characteristics. Recently, Pouretedal et al. employed controlled co-precipitation method to synthesize cubic structure of ZnS/CdS nanocomposite, and studied the photodegradation of congo red, methyl orange, methyl red and methylene blue catalyzed by prepared nanocomposites under simulated solar irradiation [12]. Jindal and Verma synthesized CdS/ZnS nanoslabs with thickness of similar to 85 nm at 160 °C using ethylenediamine as the solvent and the chelating ligand [13]. Mariappan et al. [14] and Bagdare et al. [15] deposited $Cd_{1-x}Zn_xS$ thin films by chemical bath deposition method from aqueous solution at 80 °C and after annealed at 350 and 250 °C, respectively. Panda and co-workers reported the synthesis of CdS/ZnS nanorods by a three-step solvothermal method [16], and Peng and co-workers developed a new approach (using thermal-cycling coupled single precursor) for the synthesis of CdS/ZnS nanocrystals [17]. Pandey et al. obtained ZnS/CdS quantum dots by a solution reaction while controlling the pH [18]. In addition, $Cd_{1-x}Zn_xS$ nanostructures, $Zn_xCd_{1-x}S$ solid solution, ZnS/CdS heterostructures and so on have been prepared by various methods including vapor-phase synthesis [19], single precursor reaction [20] and microwave-assisted synthesis [21]. However, complex conditions seem to be required for the above synthetic methods.

Low-temperature solid-state synthesis is an effective approach to obtain nanoparticles [22]. Comparing with gas phase [23] or liquid phase synthesis [24], it exhibits many advantages such as solvent-free, simplicity, low cost, and so on [22]. The method has been extensively used in the synthesis of many nanomaterials [25–28]. In previous work, CdS and ZnS nanoparticles were synthesized via a low-temperature heat-treatment method in the

* Corresponding author. Tel.: +86 25 84895871; fax: +86 25 84895871.
E-mail address: jsliu@nuaa.edu.cn (J. Liu).

0925-8388/$ – see front matter © 2011 Elsevier B.V. All rights reserved.
doi:10.1016/j.jallcom.2011.07.002

Table 1
The products obtained under different conditions.

Reactants	Mol value	Time (h)	Temperature (°C)	Samples
	1:2.5:1		60	CZ-60
	1:2.5:1		90	CZ-90
$Cd(CH_3COO)_2{\cdot}2H_2O$: TAA: $Zn(CH_3COO)_2{\cdot}2H_2O$	1:2.5:1	1	120	CZ-120
	1:3.5:2		60	CZ-60-2
	1:5.5:4		60	CZ-60-4
	1:2.5:1		60	ZC-60
	1:2.5:1		90	ZC-90
$Zn(CH_3COO)_2{\cdot}2H_2O$: TAA: $Cd(CH_3COO)_2{\cdot}2H_2O$	1:2.5:1	1	120	ZC-120
	1:3.5:2		60	ZC-60-2
	1:5.5:4		60	ZC-60-4

presence of surfactant. The optical properties of the products were studied, and the results show they were improved compared with bulk materials [29,30]. In addition, the synthetic routes, types, characterizations, and mechanisms of low-temperature solid-state synthetic methods for the metal oxides and sulfides nanomaterials have been reviewed [31]. However, ZnS–CdS and CdS–ZnS alloy nanoparticles synthesized through low-temperature solid-state reactions have been rarely reported.

In this study, CdS–ZnS and ZnS–CdS alloy nanoparticles were fabricated by a simple low-temperature solid-state approach. The optical properties of the CdS–ZnS and ZnS–CdS alloy nanoparticles are better than that of CdS or ZnS bulk.

2. Experimental

2.1. Materials

Cadmium acetate dihydrate [AR grade, $Cd(CH_3COO)_2{\cdot}2H_2O$], thioacetamide [AR grade, CH_3CSNH_2], zinc acetate dihydrate [AR grade, $Zn(CH_3COO)_2{\cdot}2H_2O$], and PEG-400 [polythyleneglycol, MW = 400] were purchased from Shanghai Chemical Reagent Company (China).

2.2. Synthesis of CdS–ZnS nanoparticles

Various CdS–ZnS nanoparticles were prepared using a simple solid-state reaction procedure. In a typical experiment, $Cd(CH_3COO)_2{\cdot}2H_2O$ (0.001 mol, 0.2665 g) was ground for 5 min and then mixed with PEG400 (10 mL). An appropriate amount of CH_3CSNH_2 was then added. The mixture was ground for 15 min in an agate mortar, and the appropriate amount of $Zn(CH_3COO)_2{\cdot}2H_2O$ was subsequently added to it. The resulting mixture was heated for 1 h at different temperatures in an oven after 15 min of grounding. The products were washed several times with distilled water. Finally, the obtained solids were dried in air.

2.3. Synthesis of ZnS–CdS nanoparticles

A series of ZnS–CdS nanoparticles were prepared using a procedure as similar to the above, the sequence of adding $Cd(CH_3COO)_2{\cdot}2H_2O$ and $Zn(CH_3COO)_2{\cdot}2H_2O$ was reversed. In a typical experiment, $Zn(CH_3COO)_2{\cdot}2H_2O$ (0.001 mol, 0.2195 g) was mixed with PEG400 (10 mL). After 5 min of grinding, the appropriate amount of CH_3CSNH_2 was added to the mixture. The mixture was ground for 15 min, and the appropriate amount of $Cd(CH_3COO)_2{\cdot}2H_2O$ was added to it. The resulting mixture was heated for 1 h at different temperatures in an oven after 15 min of grounding. The products were washed several times with distilled water. Finally, the obtained solids were dried in air. (The entire procedure is summarized in Table 1).

2.4. Characterization

X-ray powder diffraction (XRD) was carried out on a bruker D8-advance X-ray diffractometer with Cu-Kα radiation (λ = 0.154178 nm). Transmission electron microscopy (TEM) was performed using an FEI Tecnai-20 transmission electron microscopy with an accelerating voltage of 200 kV. Fourier transform infrared (FT-IR) spectra were obtained using a NEXUS-670 FT-IR spectrometer. Ultraviolet–visible (UV–vis) absorption spectra were obtained on an Hp-6010 spectrometer, using samples dispersed in alcohol at room temperature. Photoluminescence (PL) spectra were recorded using a Varian Cary-Eclipse spectrometer.

3. Results and discussion

The crystallinity and phase of the products were confirmed by X-ray diffraction. Fig. 1 shows the XRD patterns of CdS–ZnS and ZnS–CdS nanoparticles obtained at different temperatures. In contrast to the standard diffraction peaks, the products are not consistent with CdS or ZnS. The diffraction peaks gradually shift from ZnS to CdS with a decrease of reaction temperature, showing that the resultants are not a mixture of ZnS and CdS but CdS–ZnS and ZnS–CdS alloy materials.

According to the Scherrer equation,

$$d = \frac{k\lambda}{B\cos\theta}$$

in which d is the diameter of the crystalline core of the particles, k is a constant, λ is the wavelength of X-rays used, B is the corrected FWHM of the peak, and θ is the angle of diffraction. The particle diameter of the products CZ-60, CZ-90, CZ-120, ZC-60, ZC-90, and ZC-120 were found to be 2.1, 2.3, 2.9, 2.1, 2.3, and 2.9 nm, respectively. The diameter of the nanoparticles increased with increasing reaction temperature. The reaction sequence in the synthesis process does not appear to have any effect on the size of the nanoparticles under the same temperature.

To obtain further information on the crystalline structure, the temperature-XRD angle curves of the CdS–ZnS and ZnS–CdS alloy nanoparticles were constructed (Fig. 2). Based on the XRD results and lactic distance formulas of the cubic crystal structure, the lactic constants of CdS–ZnS and ZnS–CdS alloy nanoparticles are almost

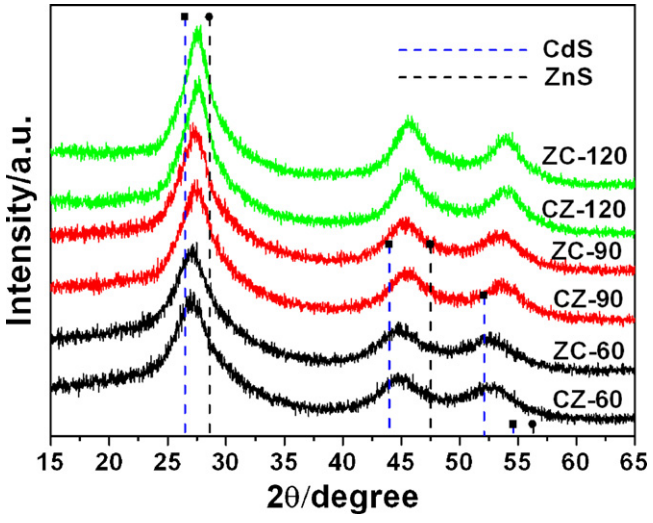

Fig. 1. XRD patterns of CdS–ZnS and ZnS–CdS alloy nanoparticles obtained at different temperatures ($Cd^{2+}/Zn^{2+} = 1$).

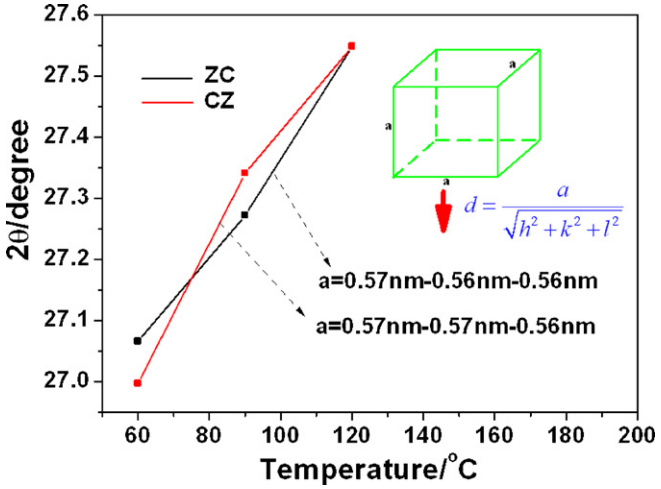

Fig. 2. Temperature–diffraction angle curves of CdS–ZnS and ZnS–CdS alloy nanoparticles ($Cd^{2+}/Zn^{2+} = 1$).

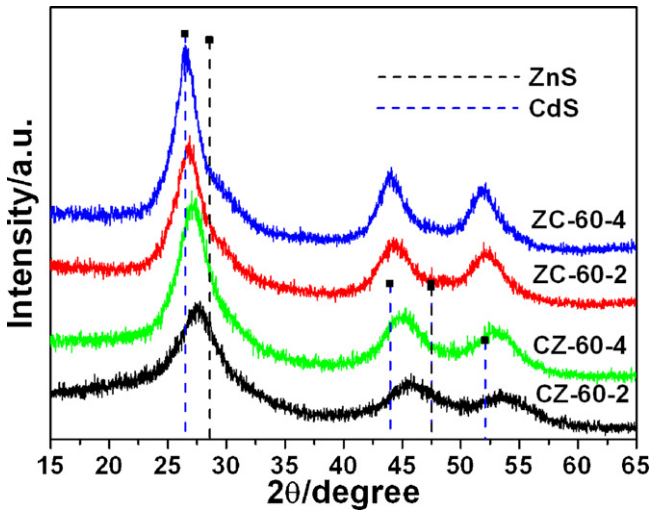

Fig. 3. XRD patterns of CdS–ZnS and ZnS–CdS nanoparticles obtained under different Cd^{2+}/Zn^{2+} and Zn^{2+}/Cd^{2+} molar ratios at 60 °C.

the same at different temperatures. This indicates that the alloy nanoparticles possess good stability.

Fig. 3 shows the XRD patterns of the CdS–ZnS and ZnS–CdS nanoparticles obtained under different Cd^{2+}/Zn^{2+} molar ratios at 60 °C. The products were identified as CdS–ZnS and ZnS–CdS alloy nanoparticles by comparison against the standard diffraction peaks of CdS and ZnS. From the Scherrer equation, the diameters of the products CZ-60-2, CZ-60-4, ZC-60-2, and ZC-60-4 were found to be 2.0, 1.9, 3.0, and 3.3 nm, respectively. The particle diameters of the CdS–ZnS products decreased gradually with increasing Cd^{2+}/Zn^{2+} molar ratios, and the diameters of the ZnS–CdS products increased gradually with increasing Zn^{2+}/Cd^{2+} molar ratios. These changes may have affected their optical properties.

From the TEM micrographs (see Fig. 4), one can see that the products consist of small spheres with different diameters. The particles size could be easily controlled by tuning the temperatures. The agglomeration of particles may result from the small dimensions and high surface energy of the particles. The FT-IR absorption spectra of the products (Fig. 5) are similar. The absorption bands attributed to the C–OH vibrations of PEG-400 are located at about 1160 and 1000 cm^{-1}, and the strong broad absorption centered at about 3460, 1620, and 1440 cm^{-1} is due to the asymmetric stretching vibrations of water.

The procedure described here involves the formation of CdS–ZnS and ZnS–CdS nanoparticles by applying a simple solid-state process. Based on the above experiments, a possible growth mechanism is proposed. Grinding of $Cd(CH_3COO)_2{\cdot}2H_2O$, TAA, and $Zn(CH_3COO)_2{\cdot}2H_2O$ in the presence of PEG400 may provide the reactant molecules with higher probability of contact [32]. A small quantity of crystalline water may be released from the structure of the molecules to form a layer of liquid film over the particles, which form a micro-aqueous environment for dissolving the TAA. When the mixture was heated, Cd^{2+} or Zn^{2+} reacted with H_2S obtained by reaction between TAA and the crystalline water, and formed CdS–ZnS and ZnS–CdS nanoparticles.

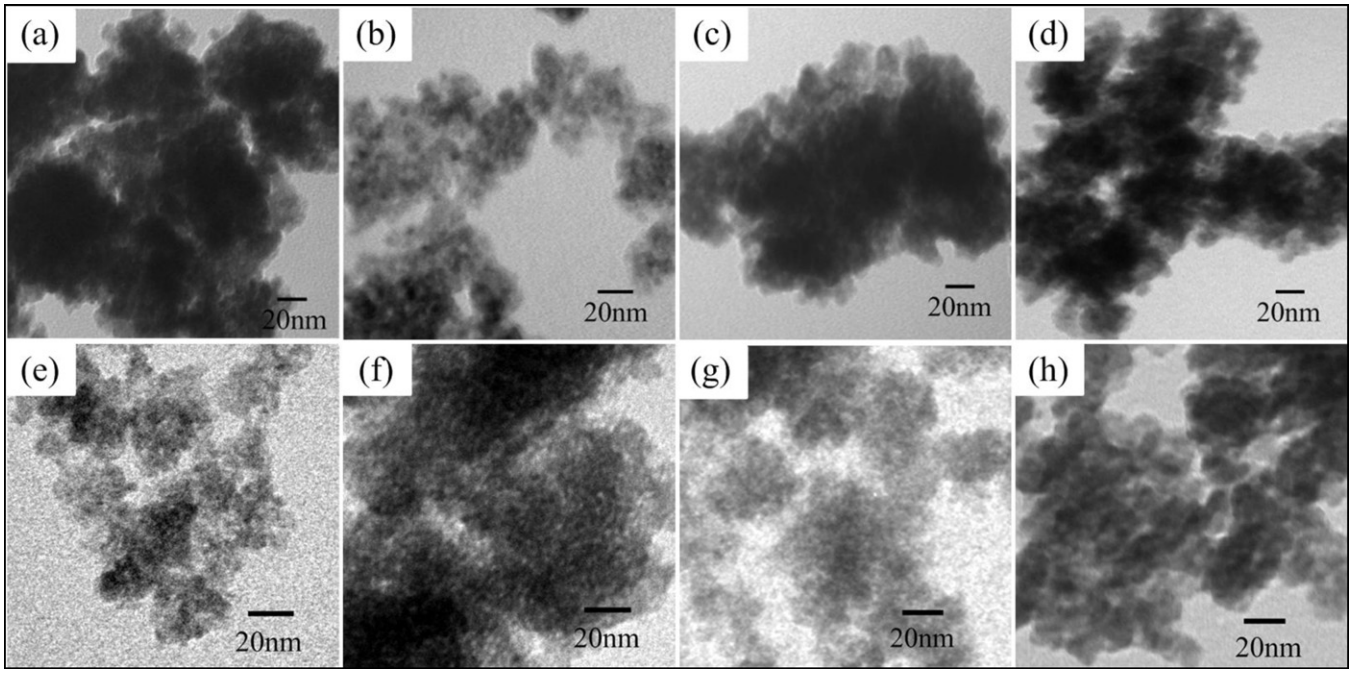

Fig. 4. TEM micrographs of the products: CZ-60(a), CZ-120(b), ZC-60(c), ZC-120(d), CZ-60-2(e), CZ-60-4(f), ZC-60-2(g), ZC-60-4(h).

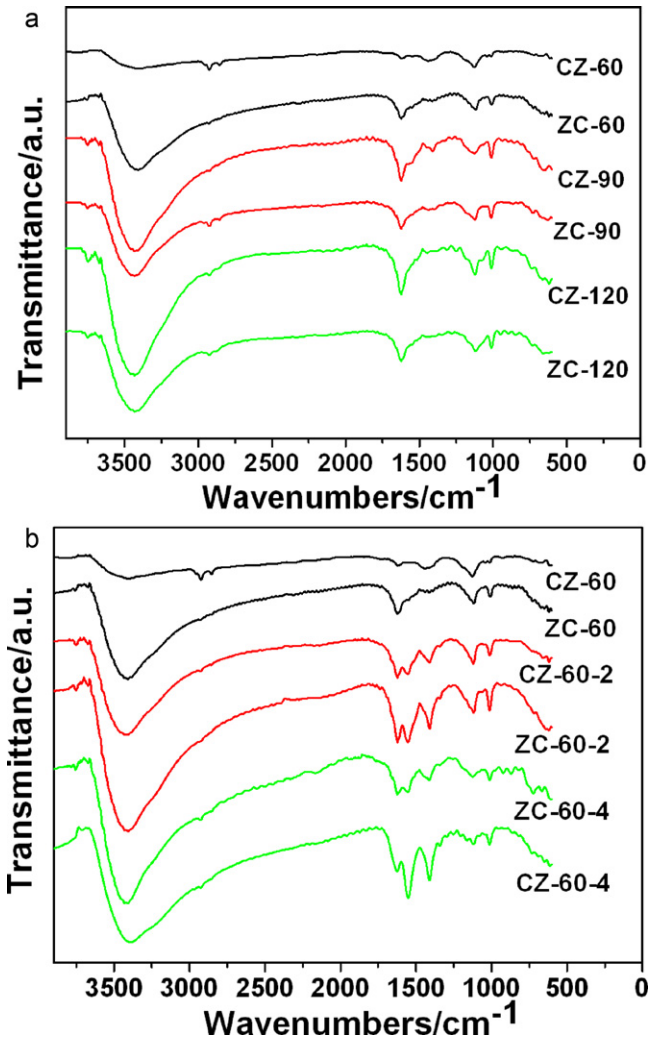

Fig. 5. FT-IR absorption spectra of the products.

The nanostructures were also studied by UV–vis spectroscopy. Fig. 6 depicts a series of UV–vis absorption spectra of the CdS–ZnS and ZnS–CdS alloy nanoparticles obtained under different temperatures with $Cd^{2+}/Zn^{2+} = 1$. The results show distinct exciton

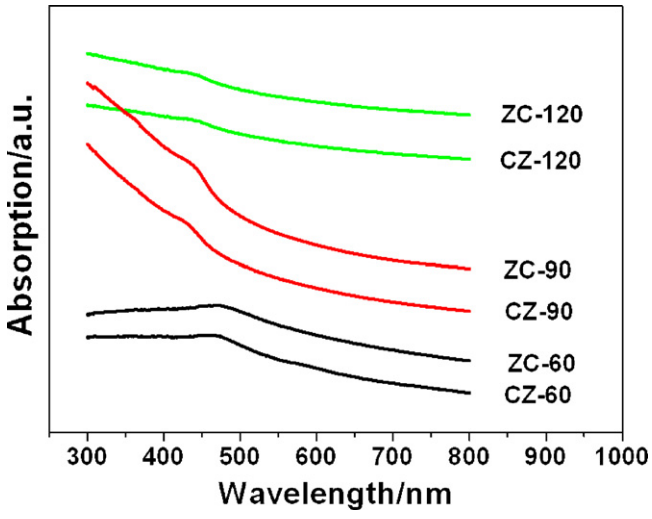

Fig. 6. UV–vis absorption spectra of CdS–ZnS and ZnS–CdS alloy nanoparticles obtained under different temperatures with $Cd^{2+}/Zn^{2+} = 1$.

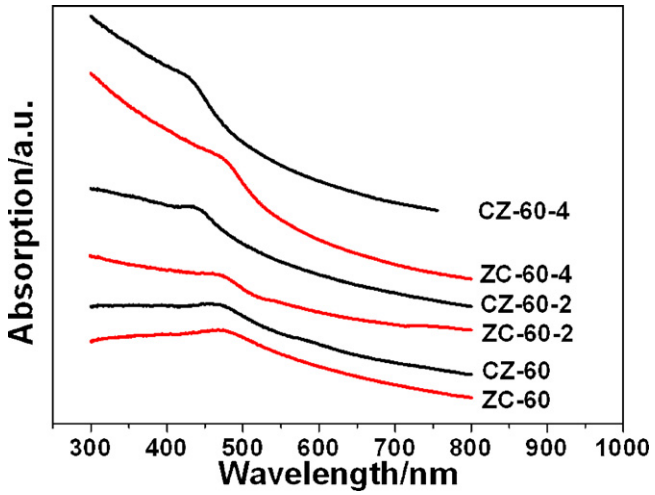

Fig. 7. UV–vis absorption spectra of CdS–ZnS and ZnS–CdS nanoparticles obtained under different Cd^{2+}/Zn^{2+} at 60 °C.

absorption. The UV–vis excitonic peaks of CZ-60, ZC-60, CZ-90, ZC-90, CZ-120, and ZC-120 are at 460, 475, 430, 440, 435, and 445 nm, respectively. The corresponding band gap energy at the maximum absorption wavelength λ_{max} for all the samples could be determined using the equation below:

$$E_g = \frac{hc}{\lambda_{max}}$$

where h is the Planck's constant, c is the light speed, and E_g is the absorption band gap. The bandgaps of CZ-60, ZC-60, CZ-90, ZC-90, CZ-120, and ZC-120 were found to be 2.70, 2.61, 2.88, 2.82, 2.85, and 2.79 eV, respectively. Compared with the peaks of the bulk CdS (510 nm, 2.42 eV) and ZnS (336 nm, 3.68 eV) crystals [33,34], the edge absorptions of the CdS–ZnS and ZnS–CdS nanoparticles are located between those of the ZnS and CdS, and depend on the reaction temperature. This confirms the formation of the alloys.

Relative to the UV–vis spectra of the CZ-60 and CZ-90, the excitonic absorption peaks show the distinct blue shift of 30 nm as the reaction temperature increases. The shift decreased when the temperature increased to 120 °C. The same change was observed for the ZC-60, ZC-90, and ZC-120. Under the same temperature, the absorption edges recorded for CdS–ZnS are blue shifted with respect to the corresponding band edges of ZnS–CdS. The absorption onsets for CdS–ZnS and ZnS–CdS are close to the corresponding onsets for ZnS and CdS, respectively. The absorbance at the peak maximum is practically dependent on the reaction temperature and reaction sequence.

From the Fig. 7, we can observe that UV–vis optical absorption excitonic peaks of CZ-60, ZC-60, CZ-60-2, ZC-60-2, CZ-60-4, and ZC-60-4 are at 460, 475, 435, 470, 430, and 470 nm, respectively. Compared with the UV–vis spectra of the CZ-60, CZ-60-2, and CZ-60-4, it can be seen that the excitonic absorption peaks show the distinct blue shift as the content of ZnS increases, while the blue shift is slight for ZC-60, ZC-60-2 and ZC-60-4. Under the same molar ratios, the absorption edges for the CdS/ZnS are blue shifted with respect to the corresponding band edges of the ZnS/CdS.

The room-temperature PL spectra (see Fig. 8) were used to investigate further the optical properties of the synthesized products. The PL spectra of CZ-120 and ZC-120 are broad and asymmetric, with an emission peak centered at ~550 nm (Fig. 8a and b). For CZ-60 and ZC-60, the center of the emission peaks is at ~590 nm. The emission peak center of CZ-90 is slightly different from that of ZC-90 (585 and 595 nm, respectively). The PL of group II–VI semiconductor materials usually consists of two emission bands at room temperature: an intrinsic near-band-edge light emission and

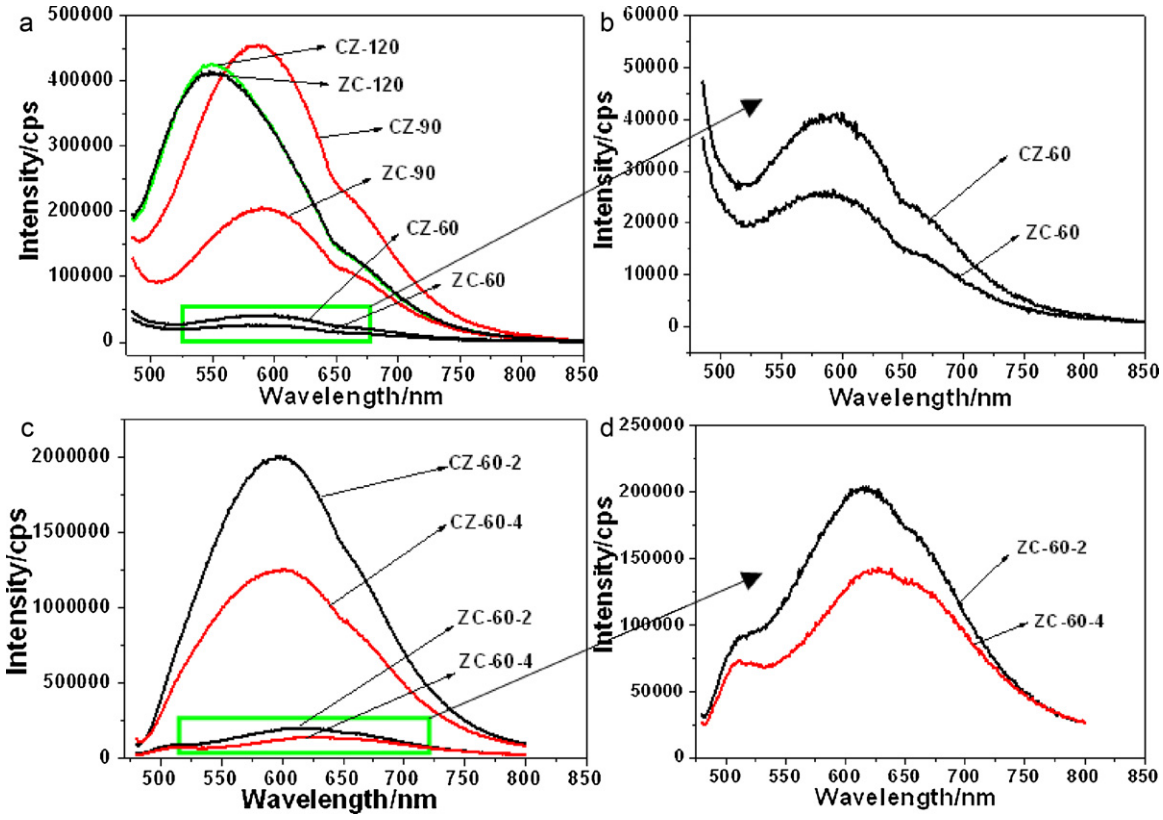

Fig. 8. PL spectra of different products synthesized under different conditions.

a broad band corresponding to the extrinsic deep-level emission in the lower energy region [35–37]. For the CdS–ZnS and ZnS–CdS nanoparticles, these strong peaks clearly come from the extrinsic deep-level emission. This might be caused by vacancy states or interstitial states of a particular nanostructure.

Comparing the PL spectra of CZ-60, CZ-90 and CZ-120, the emission peak of CZ-120 shows the distinct blue shift relative the spectra of CZ-60 and CZ-90. The same phenomenon occurred with ZC-60, ZC-90, and ZC-120. The results show that the suppression of deep-trap emission is achieved at 60 and 90 °C, resulting in the blue shift of the PL emission peak when the reaction temperature was increased to 120 °C.

Fig. 8c and d shows that the PL spectra of CZ-60-2 and CZ-60-4 are broad and asymmetric, with the emission peak centered at ~595 nm and ~600 nm, respectively. For ZC-60-2 and ZC-60-4, the centers of the emission peaks are at ~615 nm and ~625 nm, respectively. The results show that the emission peaks of samples are red shifted with increasing Cd^{2+}/Zn^{2+} or Zn^{2+}/Cd^{2+} molar ratio.

The PL intensity of the CdS/ZnS samples is larger than that of the ZnS/CdS samples under the same conditions. The increase in emission intensity may come from the different synthesis procedure in the solid-state reaction. The conduction band of the ZnS is at an energy higher than that of CdS and the valence band of the ZnS is at an energy lower than that of the CdS. The ZnS material, which has a high band gap, suppresses the tunneling of the charge carriers from the CdS to the newly formed surface atoms. Thus, more photogenerated electrons and holes are confined inside the CdS. This, consequently, passivates the nonradiative recombination sites on the surfaces and gives rise to high PL efficiency [16].

4. Conclusions

ZnS–CdS and CdS–ZnS alloy nanoparticles were synthesized using a simple low-temperature solid-state synthetic method. The XRD and TEM results show that CdS–ZnS and ZnS–CdS alloys were obtained. The size of the nanoparticles increased with increasing the reaction temperature, and the reaction sequence had no effect on the size of the nanoparticles under the same temperature. The particle diameters of the CdS–ZnS products decreased gradually with increasing Cd^{2+}/Zn^{2+} molar ratio, whereas thoes of the ZnS-CdS products increased gradually with increasing Zn^{2+}/Cd^{2+} molar ratio. The study shows that sufficient grinding and crystalline water may be a key in forming the alloy nanoparticles. The UV–vis results and PL spectra show that the optical properties of the products depend on the reaction temperature, reactant addition sequence, and reactant molar ratio.

Acknowledgments

The work is supported by Natural Science Foundation of Jiangsu Province (BK2009379), introducing talents funds of Nanjing University of Aeronautics and Astronautics (1006-909308), Nanjing University of Aeronautics and Astronautics Research Funding (1006-56Y1064), and introducing talents funds of Nanjing Institute of Technology (KXJ08138).

References

[1] X.G. Peng, M.C. Schlamp, A.V. Kadavanich, A.P. Alivisatos, J. Am. Chem. Soc. 119 (1997) 7019.
[2] S.M. Liu, H.Q. Guo, Z.H. Zhang, R. Li, W. Chen, Z.G. Wang, Phys. E 8 (2000) 174.
[3] T. Thongtem, C. Pilapong, S. Thongtem, J. Alloys Compd. 496 (2010) L29.
[4] X. Han, J. Sun, H.L. Wang, X.W. Du, J. Yang, J. Alloys Compd. 492 (2010) 638.
[5] M.A. Malik, P. O'Brien, N. Revaprasadu, Chem. Mater. 14 (2002) 2004.
[6] R.A. Caruso, M. Antonietti, Chem. Mater. 13 (2001) 3272.
[7] F. Li, Y. Jiang, L. Hu, L.Y. Liu, Z. Li, X.T. Huang, J. Alloys Compd. 474 (2009) 531.
[8] X.F. Duan, Y. Huang, R. Agarwal, C.M. Lieber, Nature 421 (2003) 241.
[9] Y.C. Zhang, G.Y. Wang, X.Y. Hu, J. Alloys Compd. 437 (2007) 47.
[10] Y.Y. Wu, H.Q. Yan, M. Huang, B. Messer, J.H. Song, P.D. Yang, Chem. A Eur. J 8 (2002) 1261.

[11] M. Navaneethan, J. Archana, K.D. Nisha, Y. Hayakawa, S. Ponnusamy, C. Muthamizhchelvan, J. Alloys Compd. 506 (2010) 249.
[12] H.R. Pouretedal, S. Sabzevari, Desalina. Water Treat. 28 (2011) 247.
[13] Z. Jindal, N.K. Verma, Phys. E-Low-Dimens. Syst. Nanostruct. 43 (2011) 1021.
[14] R. Mariappan, M. Ragavendar, V. Ponnuswamy, J. Alloys Compd. 509 (2011) 7337.
[15] P.B. Bagdare, S.B. Patil, A.K. Singh, J. Alloys Compd. 506 (2010) 120.
[16] A. Datta, S.K. Panda, S. Chaudhri, J. Phys. Chem. C 111 (2007) 17260.
[17] D.G. Chen, F. Zhao, H. Qi, M. Rutherford, X.G. Peng, Chem. Mater. 22 (2010) 1437.
[18] M. Sharma, D. Gupta, D. Kaushik, A.B. Sharma, R.K. Pandey, J. Nanosci. Nanotechnol. 8 (2008) 3949.
[19] T.Y. Zhai, X.S. Fang, H.B. Zeng, X.J. Xu, Y.S. Bando, D. Golberg, Pure Appl. Chem. 82 (2010) 2027.
[20] X. Xu, R.J. Lu, X.F. Zhao, S.L. Xu, X.D. Lei, F.Z. Zhang, D.G. Evans, Appl. Catal. B-Environ. 102 (2011) 147.
[21] H.Q. Wu, Y.Z. Yao, W.T. Li, L.L. Zhu, N. Ni, X.J. Zhang, J. Nanopar. Res. 13 (2011) 2225.
[22] Y.M. Zhou, X.Q. Xin, Chin. J. Inorg. Chem. 19 (1999) 273.
[23] J.S. Jie, G.Z. Wang, X.H. Han, J. Phys. Chem. B 108 (2004) 17027.
[24] X. Wang, Y.D. Li, J. Am. Chem. Soc. 124 (2002) 2880.
[25] Y. Chen, J.M. Zhu, X.H. Zhu, G.B. Ma, Z.G. Liu, N.B. Min, Mater. Sci. Eng. B 99 (2003) 52.
[26] Y.H. Chi, J. Zhuang, J. Yu, M.J. Tu, Chin. J. Inorg. Chem. 20 (2004) 479.
[27] T.X. Wang, H. Xiao, Y.C. Zhang, Mater. Lett. 62 (2008) 3736.
[28] Z.J. Wang, H.M. Zhang, L.G. Zhang, J.S. Yuan, S.G. Yan, C.Y. Wang, Nanotechnology 14 (2003) 11.
[29] J.S. Liu, J.M. Cao, Z.Q. Li, G.B. Ji, M.B. Zheng, J. Mater. Sci. 42 (2007) 1054.
[30] J.S. Liu, J.M. Cao, Z.Q. Li, X.F. Ke, Acta Chim. Sin. 23 (2007) 1476.
[31] J.S. Liu, Z.Q. Li, J.M. Cao, Prog. Chem. 21 (2009) 2542.
[32] Q.W. Li, G. Luo, J. Li, X. Xia, J. Mater. Process Technol. 137 (2003) 25.
[33] B. Ludolph, M.A. Malik, P. O'Brien, N. Revaprasadu, Chem. Commun. 17 (1998) 1849.
[34] N.A. Dhas, A. Zaban, A. Gedanken, Chem. Mater. 11 (1999) 806.
[35] Y.Y. Xi, T.L.Y. Cheung, H.L.N. Dickon, Mater. Lett. 62 (2008) 128.
[36] B. Cheng, W.S. Shi, J.M. Russell-Tanner, L. Zhang, E.T. Samulski, Inorg. Chem. 45 (2006) 1208.
[37] V.A. Fonoberov, A.A. Balandin, Appl. Phys. Lett. 85 (2004) 5971.